

This article was downloaded by: [University of Minnesota Libraries, Twin Cities]

On: 15 December 2013, At: 10:58

Publisher: Taylor & Francis

Informa Ltd Registered in England and Wales Registered Number: 1072954 Registered office: Mortimer House, 37-41 Mortimer Street, London W1T 3JH, UK



Aerosol Science and Technology

Publication details, including instructions for authors and subscription information:

<http://www.tandfonline.com/loi/uast20>

Mobility Analysis of 2 nm to 11 nm Aerosol Particles with an Aspirating Drift Tube Ion Mobility Spectrometer

Derek R. Oberreit^a, Peter H. McMurry^a & Christopher J. Hogan Jr.^a

^a Department of Mechanical Engineering, University of Minnesota, Minneapolis, Minnesota, USA

Accepted author version posted online: 12 Nov 2013. Published online: 13 Dec 2013.

To cite this article: Derek R. Oberreit, Peter H. McMurry & Christopher J. Hogan Jr. (2014) Mobility Analysis of 2 nm to 11 nm Aerosol Particles with an Aspirating Drift Tube Ion Mobility Spectrometer, *Aerosol Science and Technology*, 48:1, 108-118, DOI: [10.1080/02786826.2013.861893](https://doi.org/10.1080/02786826.2013.861893)

To link to this article: <http://dx.doi.org/10.1080/02786826.2013.861893>

PLEASE SCROLL DOWN FOR ARTICLE

Taylor & Francis makes every effort to ensure the accuracy of all the information (the "Content") contained in the publications on our platform. However, Taylor & Francis, our agents, and our licensors make no representations or warranties whatsoever as to the accuracy, completeness, or suitability for any purpose of the Content. Any opinions and views expressed in this publication are the opinions and views of the authors, and are not the views of or endorsed by Taylor & Francis. The accuracy of the Content should not be relied upon and should be independently verified with primary sources of information. Taylor and Francis shall not be liable for any losses, actions, claims, proceedings, demands, costs, expenses, damages, and other liabilities whatsoever or howsoever caused arising directly or indirectly in connection with, in relation to or arising out of the use of the Content.

This article may be used for research, teaching, and private study purposes. Any substantial or systematic reproduction, redistribution, reselling, loan, sub-licensing, systematic supply, or distribution in any form to anyone is expressly forbidden. Terms & Conditions of access and use can be found at <http://www.tandfonline.com/page/terms-and-conditions>



Mobility Analysis of 2 nm to 11 nm Aerosol Particles with an Aspirating Drift Tube Ion Mobility Spectrometer

Derek R. Oberreit, Peter H. McMurry, and Christopher J. Hogan, Jr.

Department of Mechanical Engineering, University of Minnesota, Minneapolis, Minnesota, USA

We describe the performance of a drift tube-ion mobility spectrometry (DT-IMS) instrument for the measurement of aerosol particles. In DT-IMS, the electrical mobility of a measured particle is inferred directly from the time required for the particle to traverse a drift region, with motion driven by an electrostatic field. Electrical mobility distributions are hence linked to arrival time distributions (ATDs) for particles reaching a detector downstream of the drift region. The developed instrument addresses two obstacles that have limited DT-IMS use for aerosol measurement previously: (1) conventional drift tubes cannot efficiently sample charged particles at ground potential and (2) the sensitivities of commonly used Faraday plate detectors are too low for most aerosols. Obstacle (1) is circumvented by creating a “sample volume” of aerosol for measurement, defined by the streamlines of fluid flow. Obstacle (2) is bypassed by interfacing the end of the drift region with a condensation particle counter. The DT-IMS prototype shows high linearity for arrival time versus inverse electrical mobility ($R^2 > 0.99$) over the size range tested (2.2–11.1 nm), and measurements compare well with both analytical and numerical models of device performance. A dimensionless calibration curve linking drift time to inverse electrical mobility is developed. In less than 5 s, it is possible to measure 11.1 nm particles, while 2.2 nm particles are analyzable on a subsecond scale. The transmission efficiency is found to be dependent upon electrostatic deposition for short drift times and upon advective losses for long drift times.

[Supplementary materials are available for this article. Go to the publisher’s online edition of *Aerosol Science and Technology* to view the free supplementary files.]

INTRODUCTION

Differential mobility analyzers (DMAs) (Knutson and Whitby 1975; Chen et al. 1998; Fernandez de la Mora and Kozlowski 2013), as well as a number of other recently developed devices (Flagan 2004; Kulkarni and Wang 2006; Zhang and Wexler 2006; Song and Dhaniyala 2007; Vidal-de-Miguel et al. 2012), can be categorized as spatial electrical mobility spectrometers, as these instruments separate continuously sampled particles in electrical mobility by directing them along mobility-dependent trajectories (mobility separation in space). Because the residence time of transmitted particles in a DMA is fixed and independent of particle size, diffusional broadening leads to degradation of instrument resolution for sub-20-nm particles (Stolzenburg 1988; Stolzenburg and McMurry 2008; Downard et al. 2011). Furthermore, instruments that use DMAs to obtain information about particle size or size distributions, such as tandem differential mobility analyzers and scanning mobility particle spectrometers, typically require several minutes to complete voltage scans (Wang and Flagan 1990). This limits information that can be obtained when aerosols are varying rapidly, such as can occur during sampling with an aircraft or near roadways.

Electrical mobility spectrometry is likewise used for the detection of gas phase ions (referred to as ion mobility spectrometry in this circumstance), which consist of <1000 atoms and have mobility equivalent diameters <2 nm (St. Louis and Hill 1990; Borsdorf and Eiceman 2006). In contrast to aerosol particle analysis, electrical mobility based analyses for ions are frequently carried out with drift tubes, in which ions, sampled at a specific time, migrate across an electrostatic gradient toward a detector, and the electrical mobility of an ion is inversely proportional to its transit time through the drift tube (mobility separation in time). DT-IMS instruments do not need to be scanned in operational parameters to measure ions with a range of electrical mobilities, as all measured entities migrate along similar trajectories toward the detector. Unsteady size/mobility

Received 12 July 2013; accepted 29 September 2013.

This work was supported by National Science Foundation Grant CHE-1011810. Derek R. Oberreit acknowledges support from a National Defense Science & Engineering Graduate (NDSEG) fellowship as well as a National Science Foundation Graduate Research Fellowship (NSF GRFP). We thank Dr. Susanne Hering (Aerosol Dynamics Inc.) for the loan of a WCPC 3788 for testing the prototype device. Finally, we acknowledge the Minnesota Supercomputing Institute (MSI) for providing support for numerical simulations.

Address correspondence to Christopher J. Hogan, Jr., Department of Mechanical Engineering, University of Minnesota, 103 Mechanical Engineering, 111 Church St. SE, Minneapolis, MN 55455, USA. E-mail: hogan@me.umn.edu

Color versions of one or more of the figures in the article can be found online at www.tandfonline.com/uast.

distributions can be examined via DT-IMS, even those that vary on timescale faster than the ion/particle drift times. Because transit time within a drift tube is inversely proportional to the diffusion coefficient of a charged particle (Mason and McDaniel 1988), instrument resolution is additionally independent of particle size in an ideal drift tube (Revercomb and Mason 1975). Moreover, to access the electrical mobilities of nanometer-sized particles with modest to high resolution (>20), DMAs require high sheath gas flows, which pose operational difficulties in maintaining laminar and steady flow (Rosser and Fernandez de la Mora 2005) and necessitate the use of electrical mobility standards for sheath flow calibration (Ude and Fernandez de la Mora 2005; Attoui et al. 2013). With these limitations DMAs rarely have resolving powers in excess of 50 (Martinez-Lozano and Fernandez de la Mora 2006); free of such restrictions, current state-of-the-art DT-IMS systems can attain resolving powers well in excess of this value (Merenbloom et al. 2009).

However, the application of DT-IMS for measurements of aerosol particles >2.0 nm in size remains unexplored, because of several limitations in current instrument designs. First, many DT-IMS systems operate at reduced pressure (several Torr) and require that analytes (vapor phase species or particles) be ionized within the inlet region at high potential. Existing DT-IMS systems are hence incapable of sampling charged species from atmospheric pressure environments at or near ground potential without substantial electrostatic particle deposition. Second, DT-IMS instruments commonly employ low sensitivity, fast response Faraday plate detectors internal to their drift regions and cannot be readily coupled with aspirating, single particle detectors (i.e., condensation particle counters, CPCs), leading to the requirement that analyte concentrations be in excess of those commonly encountered in aerosols. Third, drift times in existing DT-IMS systems are on the order of milliseconds, which is significantly faster than the response time of any existing CPC (Wang et al. 2002). Therefore, even if an existing DT-IMS instrument was modified to couple with an aspirating detector, CPC response times would prohibit measurement.

The advantages of DT-IMS suggest that a suitable DT-IMS instrument for aerosol analysis would find application in a number of instances (e.g., determination of size distribution functions in turbulent flows). We have hence constructed a prototype DT-IMS instrument that overcomes the aforementioned obstacles in implementation for aerosol particles. In subsequent sections, the design of the prototype DT-IMS instrument is described in detail, as are measurements of DMA-classified aerosol particles with the prototype instrument coupled to a CPC. Analytical models and a combined Eulerian–Lagrangian simulation approach are used to predict particle transport through the instrument, and are compared to measurements. We show that with the prototype DT-IMS device, it is possible to analyze particles in the 2.2–11.1 nm size range with measurement times ranging from 15 s down to subsecond scales (with longer times and larger sizes are also analyzable).

EXPERIMENTAL AND THEORETICAL METHODS

DT-IMS Prototype Overview

A labeled schematic of the prototype DT-IMS is shown in Figure 1a (cross-sectional view), with a rendered cutaway image shown in Figure 1b. Calculated flow streamlines at the inlet and outlet (with calculations described in the online supplementary information [SI]), are depicted in Figures 2a and b, respectively. Lines of isopotential (electrostatic), formed when voltage is applied for measurement, are also shown in Figures 2a and b, as well as in Figure 2c for the entire device. We concurrently refer to Figures 1a and b and Figures 2a and c in providing a general description of the DT-IMS prototype manner of operation.

During operation, aerosol is continuously directed into the “sample inlet.” The entire device is held at ground potential prior to the start of each measurement, and any particles entering the device follow the indicated “sample inlet streamlines,” i.e., entering particles traverse the “approximate sample volume,” and are then transported to the “excess outlet.” Particles do not traverse the “drift region” under these circumstances, as an additional flow, sent continuously into the device at the “counterflow inlet,” passes through the drift region from outlet to the inlet. The inlet of the DT-IMS can, therefore, be described as a fluid-mechanical gate, which is distinct from the electrostatic gating schemes employed in conventional DT-IMS instruments (Dugourd et al. 1997).

The “drift region” is a cylindrical tube consisting of a series of ring electrodes. Connected to the first ring electrode is a conducting mesh screen (labeled in Figure 1a); sample inlet streamlines pass through this mesh screen both as they enter the device, and as they leave through the excess outlet. To begin a measurement, voltage is applied to the first ring electrode and the mesh screen (noted as the “location of maximum potential” in Figure 2a), and the voltage decreases nearly linearly from electrode to electrode, leading to the electrostatic isopotential lines in Figure 2c. The trajectories of uncharged particles, both those that have already entered the “sample inlet” and those entering after the voltage is applied, are unchanged, and they continue to exit through the “excess outlet.” The sample inlet remains grounded at all times. Therefore, particles charged to the opposite polarity of the applied voltage, irrespective of whether they enter the device before or after the voltage is applied, are directed electrostatically toward the mesh screen. Conversely, particles charged with the same polarity as the applied voltage are transported in a manner dependent upon whether they enter the device prior to voltage application (and are to the right “location of maximum potential” in Figure 2a) or after voltage is applied. In the latter instance, the electrostatic potential gradient between the mesh screen and sample inlet tube directs these particles onto the sample inlet tube. In the former instance, an electrostatic force directs particles axially across the drift region. If a particle’s resulting electrophoretic velocity (the product of its electrical mobility and the axial electrical field strength) is greater than the velocity of the counterflow in the drift region,

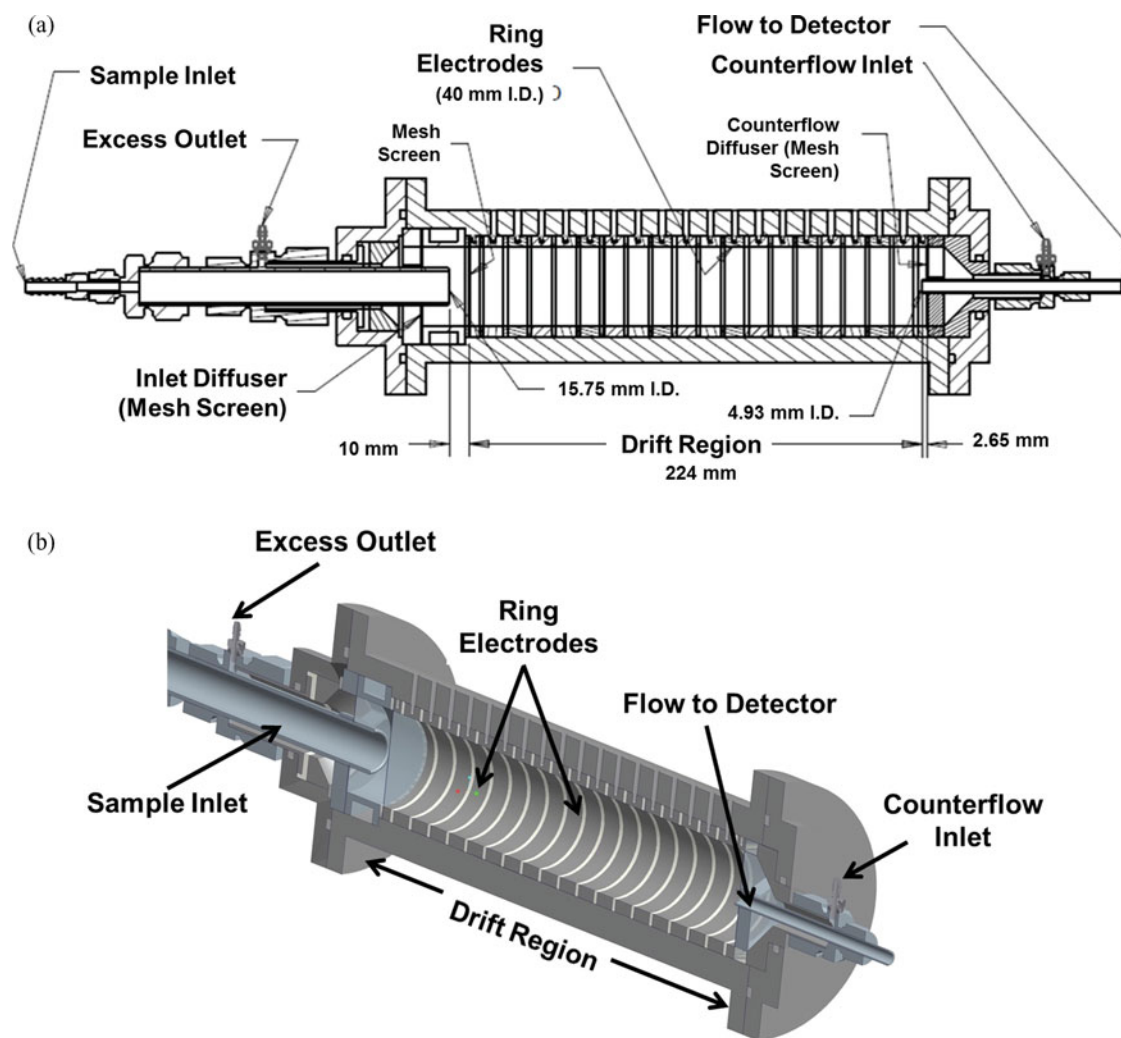


FIG. 1. (a) Schematic of the DT-IMS prototype. (b) A three-dimensional cutaway image of the DT-IMS prototype.

the particle will traverse the drift tube, with the time required to traverse the drift region (i.e., the drift time) a function of the particle's electrical mobility, Z_p . Upon traversing the drift region, particles near the center of the drift region tube are driven by fluid flow to the detector (along the "flow to detector streamlines"), and the detector (a CPC) aspirates flow out of the drift region. Particles at outer radial locations deposit diffusively and electrostatically on the device's outer walls. Additional time is required for particles to be detected, yet provided that the response time distribution of the detector is sufficiently narrow relative to the particle drift time (the time required for a particle to traverse the drift region), then the time at which a particle is detected (with zero time defined as the instant at which the voltage is first applied) is primarily a function of the electrical mobility of the particle.

A video file depicting particle trajectories through the prototype both prior to and during measurement is provided in the SI. We note that with a DT-IMS instrument operated as described,

at no point are measured particles required to travel "upstream" across electrostatic gradients, and that charged particles may be directly sampled from ground potential, atmospheric pressure aerosols. Particles, which traverse the drift region once voltage is applied, are considered to be part of the sample volume for each measurement. Although the actual size of the sample volume is electrical mobility dependent and difficult to quantify, with sufficiently small sample volumes DT-IMS instruments are capable of substantially higher time resolution measurement than their spatial mobility filter counterparts, with the time resolution related to the time required to fill the sample volume.

DT-IMS Prototype Design

A number of DT-IMS systems can be designed which operate in the aforementioned manner to separate particles of disparate electrical mobilities from one another. The dimensions of the prototype DT-IMS device presented here are provided in

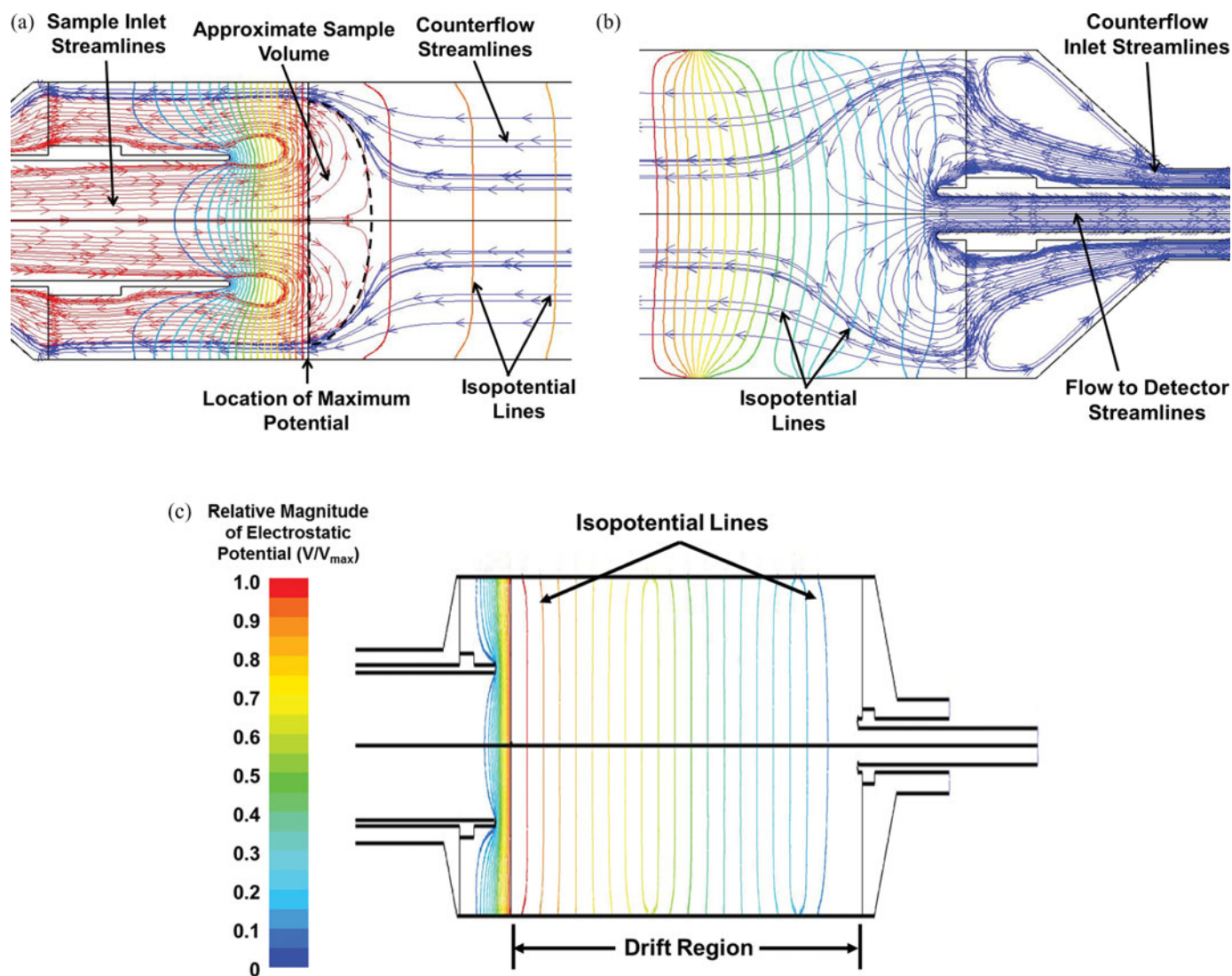


FIG. 2. Depictions of (a) the streamlines and isopotential lines at the DT-IMS prototype inlet formed by the sample inlet flow and counterflow, (b) the streamlines and isopotential lines formed by the counterflow at the prototype outlet, and (c) the isopotential lines in the drift region.

Figure 1a. Measurements are carried out with a counterflow inlet air flowrate of 0.815 l min^{-1} , and a CPC detector flowrate of 0.615 l min^{-1} (Figures 1a and 2b). Air is hence transported across the drift region (from outlet to inlet) at a net flowrate of 0.2 l min^{-1} . The excess outlet flow is regulated at 1.0 l min^{-1} , which results in a sample inlet flowrate of 0.8 l min^{-1} (excess outlet flowrate = sample inlet flowrate + counterflowrate). The cylindrical tube defining the drift region is made of nonconductive polycarbonate plastic, in which 20 stainless steel ring electrodes are fixed. The electrodes themselves are $\sim 10 \text{ mm}$ in width with $\sim 2\text{-mm}$ -wide insulating spacers between electrodes. Connected to the first electrode is a stainless mesh screen (15×15 wire mesh, $0.01''$ diameter wires, covering the entirety of the drift region cross section), which the sample flow traverses prior to exiting through the excess outlet. A voltage in the range

$1 \text{ kV} - 9 \text{ kV}$ is applied to the first electrode (higher voltages than 9 kV lead to corona discharge), while the last electrode is held at ground during measurement. A chain of equivalent value resistors ($600 \text{ k}\Omega$ for all but the final three electrodes) connects all electrodes to their immediate neighbors, creating a near constant axial electric field in the drift region, as depicted in Figure 2c. A slight nonlinearity in the voltage profile is present at the end of the drift region; the final three electrodes are connected by two resistors of lower resistance than those prior ($300 \text{ k}\Omega$ and $150 \text{ k}\Omega$, respectively). This causes a radial electric field to develop at the outlet, an effect which is expanded upon and discussed further in a forthcoming manuscript (Oberreit et al. 2013). After particles pass through the sample outlet tube, they arrive at the detector, which is a water-based condensation particle counter for the present setup (TSI model 3788 or 3786

[Hering and Stolzenburg 2005; Hering et al. 2005; Iida et al. 2008]).

DT-IMS Arrival Time Distribution Measurements

In DT-IMS, measurements are quantified via arrival time distributions (ATDs), i.e., the signal (number of particles, when using a CPC) per unit measurement time (adjustable to per unit log time, as is used in this study) as a function of measurement time. The performance of the prototype DT-IMS was tested by measuring the ATDs of DMA classified particles. A schematic of the system used for the tandem DMA-DT-IMS experiments is provided in the SI (Figure S1). The test aerosol was generated using a tube furnace generator (Lindberg Blue) as described by Scheibel and Porstendorfer (1983) with sodium chloride as the particle material. The supply gas flowrates for the furnace ranged from 3 to 5 l min⁻¹ and the set furnace temperature was ~645°C. The particle electrical mobility (diameter) window was selected using a high-resolution DMA (Nano-Engineering Corp., the half-mini DMA [Fernandez de la Mora and Kozlowski 2013]) operated in recirculating mode with a resolving power, $R \approx 36$ (determined using an electro-spray generated monomobile calibration ion, tetradodecylammonium⁺ [Ude and Fernandez de la Mora 2005]). The calibration ion was also used to determine the DMA voltage/mobility relationship and was measured at the beginning and end of each experiment. An orifice was placed downstream of the DMA to insure that the aerosol was well mixed prior to branching the flow into the DT-IMS prototype, a reference counter to monitor the inlet concentration, and an excess aerosol vent to a filter. For comparison to models, the size distribution function at the DMA outlet/DT-IMS instrument inlet was approximated as a Gaussian distribution using the measured resolving power of 36.

At the start of a measurement the DT-IMS voltage (either 1 kV, 3 kV, or 9 kV, facilitating the migration of positively charged particles) was applied to the first electrode using a high-voltage power supply (Bertan high voltage) and relay (Cynergy 3 Components Ltd.) that was switched via a data acquisition module controlled using *Labview* software (*National Instruments*). The software counts the number of digital pulses sent by the detector, which indicate detected particles, and assigns them to a time interval based on the delay between onset of the relay and the detection of the pulses. The software further facilitates the collection of multiple ATDs, which were exported and later averaged. In total, 150 bins in time were used to define ATDs. For the test results presented in this work the number of measurements was varied from 3 to 10 with higher numbers of scans chosen for lower input concentrations. Multiple measurements were employed primarily to ensure repeatability; under most operating conditions particle concentrations at the DMA outlet were high enough to allow for sufficient signal-to-noise during collection of a single ATD.

Predictions of Arrival Time Distributions (ATDs) and Simulation of Particle Trajectories

For comparison to experimental measurements, we examine DT-IMS measurements via both an analytical model and numerical simulations. As is derived in the SI, for prescribed DT-IMS operating conditions (flowrates and voltage) the ATD (for positively charged particles) can be approximated as:

$$\begin{aligned} \text{ATD}(t) &= \int_0^t [\Gamma(t_{\text{drift}})\Phi(t_{\text{det}})]dt_{\text{drift}} \\ &= \int_0^t [\Gamma(t_{\text{drift}})\Phi(t - t_{\text{drift}})]dt_{\text{drift}} \end{aligned} \quad [1a]$$

$$\Gamma(t_{\text{drift}}) = \sum_{q=1}^{q=\infty} \left[\int_0^{\infty} \eta_T \eta_A \eta_{\text{Det}} f_{q,d_p} \Theta_{\text{IMS}}(Z_p, t_{\text{drift}}) \bar{n} dd_p \right] \quad [1b]$$

$$\Phi(t_{\text{det}}) = \frac{df_{\text{det}}}{dt_{\text{det}}}, \quad [1c]$$

where t is the total measurement (arrival) time, t_{drift} is the time required for a particle to traverse the drift tube, and t_{det} is the time required for a particle, having exited the drift region, to be detected. A detected particle only contributes to the ATD at an arrival time equal to sum of its drift time and detection time; hence $t_{\text{det}} = t - t_{\text{drift}}$. Equation (1a) expresses the ATD as a convolution integral over the product of two near-independent functions: the first, $\Gamma(t_{\text{drift}})$, dependent upon the time for particles to traverse the drift tube (t_{drift}) and representing the ATD of a DT-IMS device with a perfect detector (i.e., a detector that responds at the same instant to all particles with a given t_{drift}), and the second, $\Phi(t_{\text{det}}) = \frac{df_{\text{det}}}{dt_{\text{det}}}$, the probability distribution function for the detector response times (i.e., $\Phi(t_{\text{det}})dt_{\text{det}}$ is the fraction of particles between t_{det} and $t_{\text{det}} + dt_{\text{det}}$ after they flow into the detector inlet at the exit from the drift tube). In $\Gamma(t_{\text{drift}})$, $\bar{n} dd_p$ is the number of particles in the sample volume with sizes between d_p and $d_p + dd_p$ in the sampling volume (Figure 2a and the SI), and f_{q,d_p} is the (dimensionless) fraction of particles of diameter d_p that have integer charge level q . f_{q,d_p} must be known a priori (Wiedensohler 1988; Gopalakrishnan et al. 2013), and for a given set of background gas conditions (temperature, pressure, and composition) the electrical mobility of a particle is defined exactly by its diameter and integer charge level from the Stokes-Millikan equation:

$$\begin{aligned} Z_p &= \frac{qe}{3\pi\mu(d_p + d_g)} \left(1 + \frac{2\lambda}{(d_p + d_g)} \right. \\ &\quad \left. \times \left(1.257 + 0.4 \exp \left[-\frac{0.55(d_p + d_g)}{\lambda} \right] \right) \right), \end{aligned} \quad [1d]$$

where e is the unit electron charge, λ is the gas mean-free path, d_g is the effective gas molecule diameter (0.3 nm in air near room temperature [Larriba et al. 2011]), and μ is the gas

dynamic viscosity. η_T , η_A , and η_{Det} are the transmission efficiencies of the sample inlet and drift region, drift region outlet and aspirating detector inlet, and the detector itself, respectively. These transport efficiencies are governed by particle deposition due to both diffusion and electrostatic precipitation at the counterflow screen, though we neglect electrostatic effects in the analytical model. $\Theta_{\text{IMS}}(Z_p, t_{\text{drift}})$ is the ideal drift time probability distribution function (Revercomb and Mason 1975), i.e., $\Theta_{\text{IMS}}(Z_p, t_{\text{drift}})dt_{\text{drift}}$ is the fraction of particles in the sample volume with electrical mobility Z_p , and with drift times from t_{drift} to $t_{\text{drift}} + dt_{\text{drift}}$, assuming negligible particle depositional loss during migration.

As described in the SI, the transmission efficiency into the drift region, η_T , is approximated as the product of the penetration of particles through a wire mesh screen (Cheng and Yeh 1980) and through the sample inlet tube (Gormley and Kennedy 1949). Particle losses in the drift region are not considered in the analytical model, as there is a complex relationship between electrostatic deposition and particle residence time. Similar to the sampling inlet tube, the transmission efficiency through drift region outlet and aspirating detector inlet, η_A , can be approximated with the Gormley & Kennedy equation. For calculations we neglect size-dependencies in the detector efficiency, η_{Det} , setting $\eta_{\text{Det}} = 1.0$ under all circumstances. $df_{\text{det}}/dt_{\text{det}}$ was determined experimentally for the detectors used in this study, also described in the SI.

To develop an expression for $\Theta_{\text{IMS}}(Z_p, t_{\text{drift}})$, we note that with negligible counterflow in the drift region, the square of the full width at half-maximum (FWHM) of the drift time distribution for an ideal DT-IMS instrument, $(\Delta t_{\text{drift}})^2$, is given by Revercomb and Mason (1975) as:

$$(\Delta t_{\text{drift}})^2 = (\Delta t_0)^2 + \frac{16 \ln(2)t_{\text{ave}}^2}{\Psi_E} \quad [2a]$$

where Δt_0 is the half width of the input pulse (determined by the axial length of the sample packet, as indicated in Figure 2a), Ψ_E is the electrical potential energy to thermal energy ratio (Gopalakrishnan and Hogan 2012) for the drift tube, i.e., the ratio of the product of the particle charge (qe) and the applied voltage V to the product of Boltzmann's constant, k , and the gas temperature T , and t_{ave} is the average ideal drift time ($L^*L_E / Z_p V$, where L is the drift region length, and $L_E = 22.7$ cm is electrode to electrode distance defining the electric field). The value for Δt_0 is related to the axial length of the sample volume, indicated in Figure 2a (Δx), through the equation:

$$\Delta t_0 = \frac{\Delta x L_E}{Z_p V}. \quad [2b]$$

We estimate $\Delta x \approx 0.8$ cm and correspondingly assume $L = 22$ cm (the average length of drift region considering particles begin migration $\Delta x/2$ into the drift tube) for the prototype. Equations (2a) and (2b) neglect any influence of counterflow.

Following the procedure of Revercomb and Mason (1975) with the assumption of simple plug flow acting in the drift region, the square of the FWHM of the drift time distribution becomes:

$$(\Delta t_{\text{drift}})^2 = (\Delta t_0)^2 + \frac{16 \ln(2)t_{\text{ave}}^2}{\Psi_E - Pe} \quad [2c]$$

where Pe is the Peclet number, defined as $u_c L z e / (Z_p k T)$, t_{ave} is redefined as $(L^* L_E / [Z_p V - u_c L_E])$, and Δt_0 is similarly modified to $(\Delta x L_E / ([Z_p V - u_c L_E])$. Ψ_E , the electrostatic energy to thermal energy ratio, may also be treated as the ratio of a particle's electrophoretic speed to its diffusive speed (i.e., it may be treated as an electrostatic Peclet number [Flagan 1999]), hence the parameter $\Psi_E - Pe$ is the net Peclet number for transport through the drift tube and Pe / Ψ_E is the ratio of a particle's advective speed to its electrophoretic speed (equivalent to $u_c L / (Z_p V)$). The resolving power of a DT-IMS instrument considering counterflow ($R = t_{\text{ave}} / \Delta t_{\text{drift}}$) is approximated as:

$$R = \left[\left(\frac{\Delta x}{L} \right)^2 + \frac{16 \ln(2)}{\Psi_E - Pe} \right]^{-1/2} \quad [2d]$$

and the probability distribution function for drift times, approximated as a normal distribution, is given by the equation:

$$\Theta_{\text{IMS}}(Z_p, t_{\text{drift}}) = \sqrt{\frac{2 \ln(2)}{\pi}} \frac{1}{\Delta t_{\text{drift}}} \times \exp \left(-4 \ln(2) \left[\frac{t_{\text{drift}}}{\Delta t_{\text{drift}}} - R \right]^2 \right). \quad [2e]$$

Equation (2d) reveals that a DT-IMS instrument's resolving power is limited by the finite width of its sample volume and by particle diffusion, and has a maximum value of $L/\Delta x$ even in the absence of particle diffusion. Analogously, Equation (2e) shows that the distribution of drift times becomes narrower as R increases.

In analytical modeling, peak normalized ATDs were determined by first randomly selecting a particle of specified electrical mobility (and diameter, assuming particles are singly charged only) from a distribution of particle sizes, chosen to match those used in experiments. Second, η_T and η_A were determined, and whether the selected particle reached the detector was determined stochastically using the product of these values. If the selected particle did indeed reach the detector, its drift time was randomly selected from the distribution described in Equation (2e), with all parameters needed to describe this distribution defined by the particle's electrical mobility and instrument operating conditions. The particle's residence time within the tube (16.3 cm) connecting the end of the drift region and the CPC inlet was determined by stochastically selecting the streamline (neglecting diffusion) on which a particle migrated to the detector. Assuming a fully developed laminar flow profile

within the tube, the probability, $P(r)$, of a particle traveling along a streamline at radial location r , is given by the equation:

$$P(r) = 4 \int_r^{r+\Delta r} \frac{r}{A^2} \left[1 - \frac{r}{A^2} \right] dr \quad [3]$$

where A is the tube radius, and Δr is a small differential in the radius. The time the particle resided within tubing at the outlet was calculated from the fully developed, laminar flow profile velocity at the radial location selected, and the time to reach the detector after exiting the tubing was subsequently randomly selected from the detector response time distribution, $\Phi(t_{\text{det}})$. Finally, the contribution of the selected particle to the ATD was determined by placing it into an appropriate time bin based upon the value of $t = t_{\text{drift}} + t_{\text{det}}$ (where t_{det} is the sum of the time the particle resided within the tube connecting the drift region to the CPC and the sampled detector response time). Normalized ATDs were determined by repeating this procedure for 10^4 particles, dividing the number of particles in each time bin by the log scale bin width (note $\frac{df}{dt} = \frac{1}{2.303t} \frac{df}{d\log_{10}(t)}$), and then by dividing this value by the total number of detected particles.

While the analytical model is useful for understanding device performance and to estimate the ATD for a given particle size distribution and $f_{q,dp}$, evaluation of the effects of complexities in the sample volume shape, the size distribution function variation within the sample volume, and the velocity field requires use of a numerical model. Therefore, we also determined particle drift times through a combination of fluid flow and electrostatic field simulations (with ANSYS[®] Fluent) coupled to a FORTAN Lagrangian particle tracking model. Details of the simulation method can be found in the SI. Simulations were used to examine individual particle trajectories in the drift region only (to determine t_{drift} for each modeled particle), as with analytical modeling, particle residence times within tubing were determined stochastically using Equation (3) and a detector response time was sampled from $\Phi(t_{\text{det}})$. Selected simulated particle trajectories within the prototype instrument are provided in the SI (as well as in the supplementary video file). The simulations show that at low Pe/Ψ_E values particles are more likely to deposit on the counterflow screen electrostatically, while at high Pe/Ψ_E values particles are lost in the inlet region due to advection. The influences of both electrostatic and advective motion are quantified subsequently in the discussion of particle transmission through the DT-IMS instrument.

RESULTS AND DISCUSSION

Analytical Model, Numerical Simulation, and Experimental Measurement Comparison

Figures 3a–c displays plots of analytically predicted, simulated, and experimentally measured normalized ATDs as a function of measurement time for DMA selected NaCl particle electrical mobility windows, with applied voltages of 1 kV, 3 kV, and 9 kV, respectively. For all displayed results the detec-

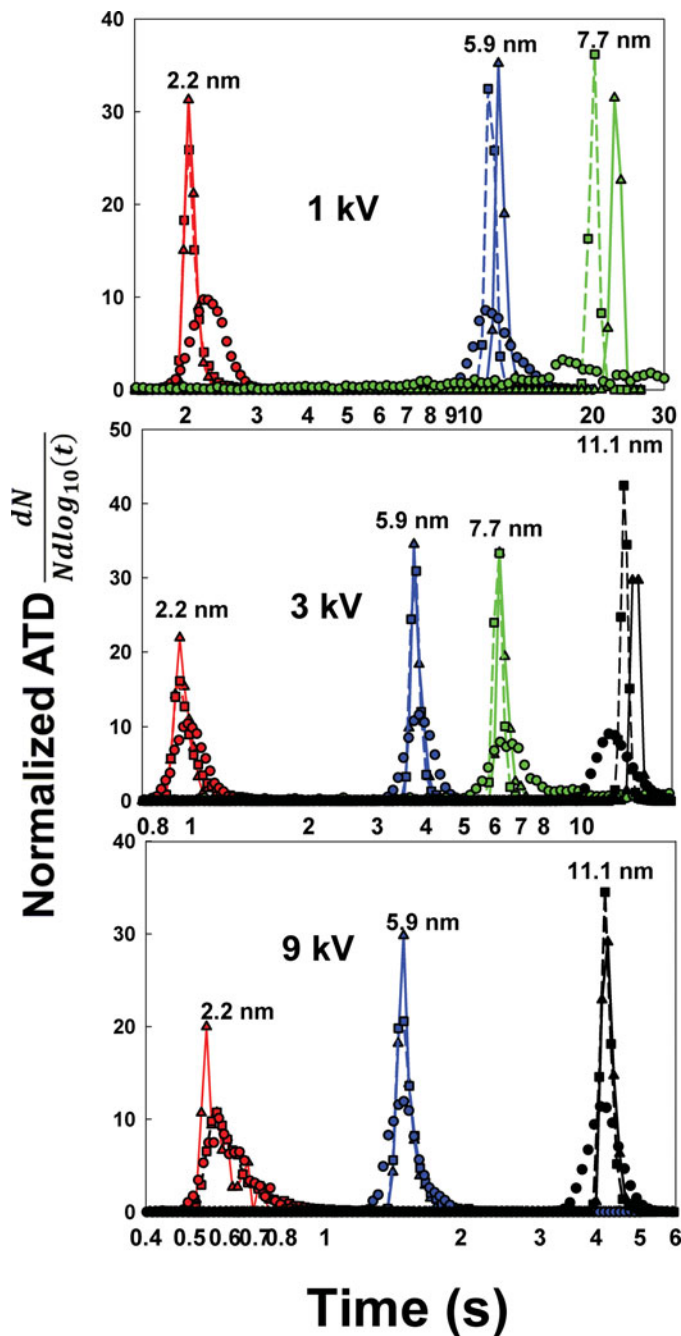


FIG. 3. Normalized arrival time distributions (dN : the number of particles per measurement bin, N : the total number of detected particles, $d\log_{10}(t)$: the log-scale bin width) as a function of measurement time, as determined from experiments (circles), simulations (triangles), and the analytical model (squares). The midpoint particle diameter (singly charged) selected by the upstream DMA is noted near the peak of each distribution.

tor was a TSI model 3788 WCPC, which has a response time distribution peaked below 0.3 s; thus, only in instances where the total measurement time is below ~ 2.0 s does the CPC response time substantially influence the distribution. Overall, strong agreement is found between analytical, simulated, and

measured ATDs, with the peak time in distributions determined by all three methods coinciding (<7%) under nearly all conditions. This demonstrates clearly that not only can the prototype DT-IMS instrument be used for the measurement of aerosol particles, but also that the prototype functions within its theoretical bounds. At the same time, however, deviations in peak location and increased FWHM for experimental ATDs as compared to the calculated distributions are evident, with deviations more pronounced at longer measurement times. We suspect this is due to slight imperfections in flow paths in the prototype device near the mesh screens, which have a more pronounced influence on particles of slower electrophoretic velocities (and hence longer drift times). Evidence supporting this is found with a nonaxisymmetric (three-dimensional) fluid flow model of the prototype device. However, we elect not to examine this deviation further here in light of the strong agreement between simulated and measured ATDs below 10 s (though it is also evident in subsequent examination of instrument resolving power).

Figure 4a is a plot of the peak measurement time in ATDs as a function of inverse electrical mobility as well as Pe for DMA-selected NaCl particles. Curves for three different applied voltages, and hence three different values of Ψ_E (for singly charged particles) are displayed. A near-linear relationship is expected for this plot provided $\Psi_E \gg Pe$. This criterion is approximately valid for all displayed conditions with the lone exception possibly at 1 kV; at the longest measurement time $Pe = 7.31 \times 10^3$ and $\Psi_E = 3.86 \times 10^4$. Correspondingly, for drift times below 10 s, the analytical, simulated, and experimentally measured curves are highly linear, with $R^2 > 0.999$ found via linear regression for all three result sets. When the normalized peak time ($\tau = tu_c/L$) is plotted as function of parameter Pe/Ψ_E , as is shown in Figure 4b, all results (both experimental and numerical) collapse to a single curve, described by the equation:

$$\tau = 1.127 \frac{Pe}{\Psi_E} + 0.0047 \quad R^2 = 0.998. \quad [4]$$

For a given set of instrument flowrates, such collapse is expected, as Pe/Ψ_E is inversely proportional to the electrophoretic velocity of particles within the drift region and all data were collected with a constant advective (counterflow) velocity profile. Equation (4) specifically applies for the experimental data below 12 s, for which $\Psi_E \gg Pe$ is approximately satisfied and for which the average deviation in electrical mobility for the measured, simulated, and analytical values compared to the values obtained from Equation (4) is 4.8%. The additional value of 0.0047 results from particle transit time to the detector, and is thus tubing length and detector dependent, while the coefficient 1.127 would vary with changing flow conditions in the drift region. However, with the prototype operated as described here, Equation (4) can be used as a calibration curve for DT-IMS measurements, directly linking the midpoint electrical mobility of detected particles to the measurement time, drift region length, and applied voltage for $Pe/\Psi_E < 0.1$.

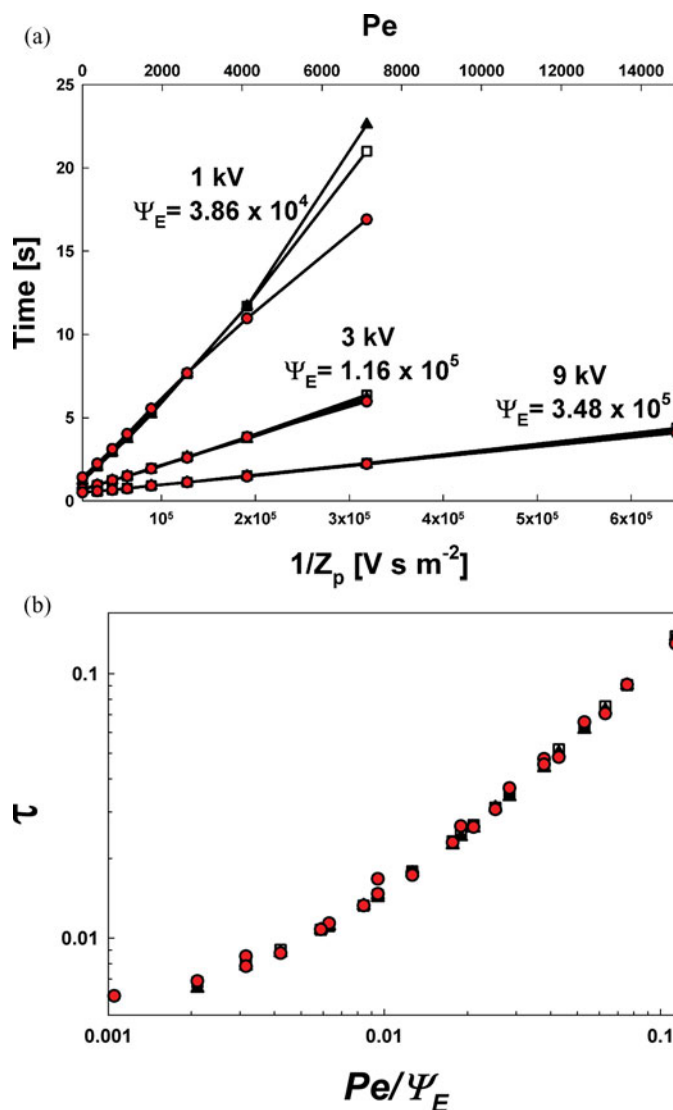


FIG. 4. (a) Peak time in ATDs as a function of inverse mobility for DMA size selected particles from experiments (circles), simulations (triangles), and the analytical model (squares). (b) Dimensionless peak time as a function of Pe/Ψ_E .

Simulated and Experimentally Measured Transmission Efficiency

The transmission efficiency of the DT-IMS instrument was also examined via both experiments and numerical simulations. The number detected per unit inlet concentration is appropriately nondimensionalized by the sample volume. However, as noted prior, the sample volume itself is difficult to estimate, and further is dependent on a number of instrument-operating parameters, most of which remained fixed in the instrument. Therefore, we opt to quantify transmission efficiency dimensionally, by plotting the total number of detected particles per unit inlet concentration as a function of Pe/Ψ_E in Figure 5, with results from both simulations and experiments shown. In the absence of losses, the value on the ordinate in Figure 5, with

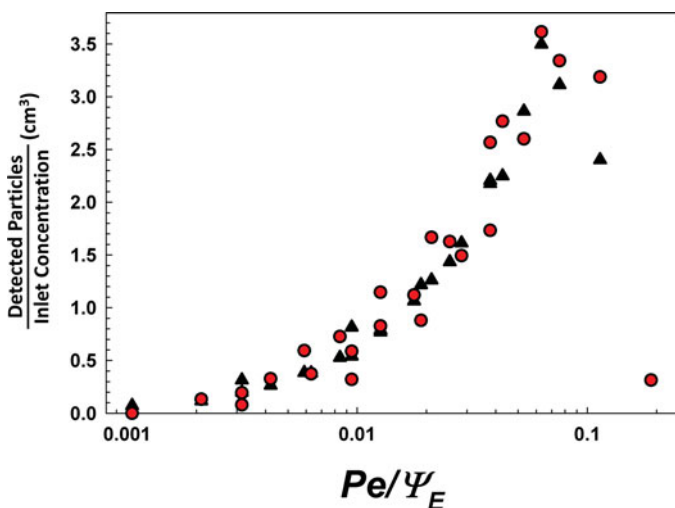


FIG. 5. The number of detected particles during a measurement per unit inlet concentration as a function of Pe/Ψ_E . Circles show measured values and triangles show simulated results.

units of volume, is a measure of the sample volume size, and the measured values are reasonable compared with the sample volume width of 0.8 cm assumed in the analytical model (the sample volume would be a 1.55 cm^3 disk based upon the inner diameter of the sample inlet tube). Experimental data and simulation results are in excellent agreement with one another, and both again collapse to a curve dependent on Pe/Ψ_E , displaying a clear maximum about $Pe/\Psi_E \approx 0.08$, near the value above which nonlinearity in the measurement time-inverse electrical mobility curve is evident. For values of this ratio below 0.1, the transmission efficiency of particles is heavily influenced by electrostatic deposition at the counterflow screen (examples visible in Figure S4). For high-concentration aerosols, where losses do not prohibit measurement, this effect can also be beneficial to resolution, as the detector preferentially samples particles which have traversed the drift region near the axis, limiting plume spreading due to the flow profile. Conversely, $Pe/\Psi_E > 0.1$ results in particle losses at the drift region inlet (also visible in Figure S4 for the 10 nm, 1 kV example).

Resolving Power

The resolving power introduced in the analytical model describes the variation in drift time for perfectly monodisperse particles entering the inlet. However, this value alone does not reflect the resolution attained during a measurement, as in its calculation variations in counterflow velocity in the drift region (spatial), transit time through tubing, and transit time within the detector are not considered. In order to quantify the total resolving power of the prototype when coupled to a specific detector, we infer the value $R_{\text{sys}} = (Z_{p,\text{peak}}^{-1})/(\Delta(Z_p^{-1}))$. This is accomplished by first fitting normalized ATDs to Gaussian distributions (described by a mean value and variance, and determined neglecting the tails within ATDs as well as Poisson weighting distributions [Kemmer and Keller 2010]), and then converting

Gaussian distributions to an inverse mobility scale (based on calibration), with mean value $Z_{p,\text{peak}}^{-1}$ and FWHM $\Delta(Z_p^{-1})$. The fitting procedure was performed for measured, simulated, and analytical results using both WCPC models 3786 and 3788, whose average response times (neglecting the tubing connect the drift region to the CPC inlet) are 280 and 850 milliseconds, respectively, with response time distribution FWHM of 50 and 210 milliseconds, respectively.

Measured, simulated, and analytical values of R_{sys} with WCPC models 3786 and 3788 are shown as functions of Pe/Ψ_E in Figure 6a and b, respectively. In calculating resolving powers we assume that the contribution of the DMA transfer function width is negligible (i.e., DMA-selected particles with a resolving power of 36 are effectively monodisperse). Additionally shown are the resolutions calculated from simulation results neglecting the influences of the detector. As evidenced by Equation (2d)

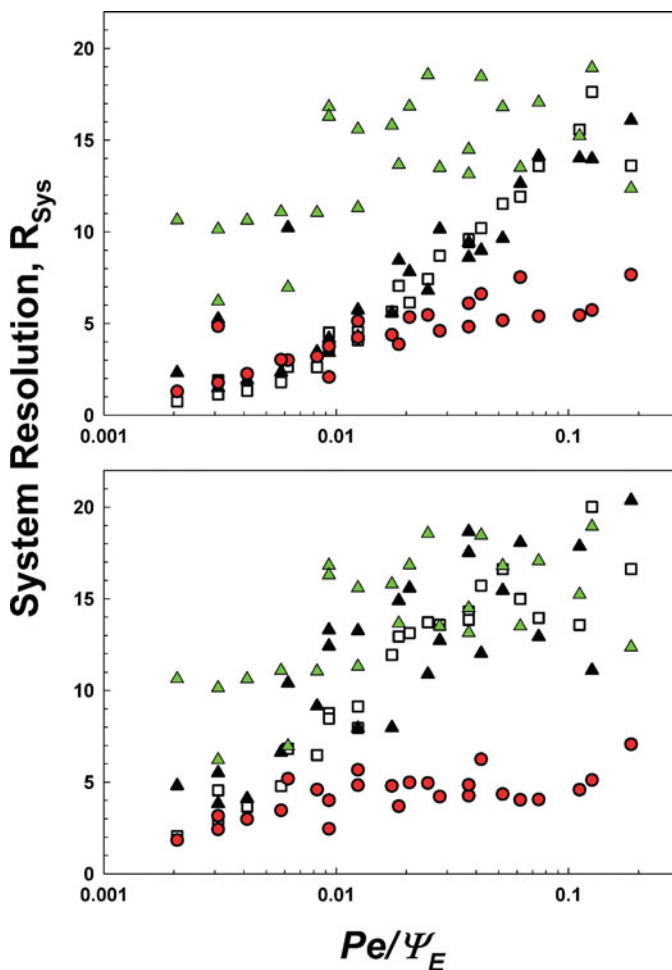


FIG. 6. The system resolving power for the DT-IMS prototype determined with (a) a 3786 WCPC and (b) a 3788 WCPC used as detectors. Circles correspond to measured values, triangles (black) to simulation results, triangles (green/gray) to simulation results neglecting detector influences, and squares to analytical results. The scatter in the calculated results reflects the finite number of particles that were tracked numerically.

directly, R_{sys} for the drift region alone is not a function of Pe/Ψ_E alone, as the resolving power of the drift region is expected to be determined by $\Psi_E - Pe$. Nonetheless, results are plotted in this manner because (1) Equation (2d) predictions suggest that resolution for the prototype instrument is more dependent on $\Delta x/L$, and (2) the other influences on R_{sys} are those that also influence transmission, and are approximately dependent on Pe/Ψ_E . Fluctuations in both the analytically calculated and simulation inferred resolving powers are evident, which result from the fact that both models utilize stochastic particle sampling to construct ATDs, and because obtained ATDs are not purely Gaussian distributions. Even so, Gaussian fitting reveals that system resolution increases with increasing Pe/Ψ_E , which correspondingly indicates that system resolution increases with increasing drift time. Evidenced by the higher resolving powers found for results of simulations without including the influence of the detector, as well as the difference in resolving power found with the model 3788 and 3786, a substantial improvement in resolution at low Pe/Ψ_E values can be made through the use of a narrow response time distribution detector. This differs from the manner in which resolution is improved in DMAs and in drift tubes used in gas phase ion measurement, which is by increasing Ψ_E (Revercomb and Mason 1975; Flagan 2004). We note finally, for the measured distributions, as Pe/Ψ_E increases, deviations from analytical and simulated results are apparent. This is further indicative of flow nonuniformities detected in nonaxisymmetric simulations, which can be rectified through prototype modification. For the size range examined (< 10 nm), however, the measured drift tube resolving power is on par with that of the TSI nano-DMA model 3085 (Chen et al. 1998).

CONCLUSIONS

A drift tube ion mobility spectrometer for measurement of aerosol particles has been developed, and the instrument's performance has been analyzed by experimental, theoretical, and numerical means. The arrival times and transmission efficiency of the device are shown to be a function of the ratio of the dimensionless parameters Ψ_E and Pe . Comparison of arrival time distributions between models and measurements support the efficacy of these models for estimating device performance for drift times less than ~ 10 s. At longer drift times predictions for ATDs diverge from measurements, and the measured resolving power of the device falls well below the predicted resolving power. Better agreement between the simulated and measured ATDs can likely be achieved by improvements to the flow diffusers used to distribute the flow evenly within the device. Further improvements to the design may include shortening the inlet and outlet regions to minimize diffusion losses as well as reduce time-based broadening, and use of a detector with a narrower response time distribution function. The advantages of the DT-IMS for particle analysis over traditional devices include relatively fast measurement times and insensitivity to changing aerosol conditions throughout the measurement period. Addi-

tionally the DT-IMS is ideally suited to be placed downstream of a DMA for tandem electrical mobility measurements, as the DMA-DT-IMS combination is the electrical mobility analog of a quadrupole mass filter-time of flight mass spectrometer (both system utilize narrow pass filters followed by time-based spectrometers). To date, our work has focused on analyses that allow measurement of size and size change. Additional work will be required to assess number distributions of the sampled aerosol, although in principle this is possible.

SUPPLEMENTARY INFORMATION

A schematic of the system used in experiments, further description of Equation (1a), a description of transmission of particles through mesh screens and tubing, a description of the CPC response time distribution measurements, a description of the numerical simulations employed, depictions of particle trajectories from simulations, and a video depiction of particle trajectories through the DT-IMS instrument are all available online.

REFERENCES

- Attoui, M., Paragano, M., Cuevas, J., and Fernandez de la Mora, J. (2013). Tandem DMA Generation of Strictly Monomobile 1–3.5 nm Particle Standards. *Aerosol Sci. Technol.*, 47:499–511.
- Borsdorf, H., and Eiceman, G. A. (2006). Ion Mobility Spectrometry: Principles and Applications. *Appl. Spectrosc. Rev.*, 41:323–375.
- Chen, D. R., Pui, D. Y. H., Hummes, D., Fissan, H., Quant, F. R., and Sem, G. J. (1998). Design and Evaluation of a Nanometer Aerosol Differential Mobility Analyzer (Nano-DMA). *J. Aerosol Sci.*, 29:497–509.
- Cheng, Y. S., and Yeh, H. C. (1980). Theory of a Screen-Type Diffusion Battery. *J. Aerosol Sci.*, 11:313–320.
- Downard, A. J., Dama, J. F., and Flagan, R. C. (2011). An Asymptotic Analysis of Differential Electrical Mobility Classifiers. *Aerosol Sci. Technol.*, 45:727–739.
- Dugourd, P., Hudgins, R. R., Clemmer, D. E., and Jarrold, M. F. (1997). High-Resolution Ion Mobility Measurements. *Rev. Sci. Instrum.*, 68:1122–1129.
- Fernandez de la Mora, J., and Kozlowski, J. (2013). Hand-Held Differential Mobility Analyzers of High Resolution for 1–30 nm Particles: Design and Fabrication Considerations. *J. Aerosol Sci.*, 57:45–53.
- Flagan, R. C. (1999). On Differential Mobility Analyzer Resolution. *Aerosol Sci. Technol.*, 30:556–570.
- Flagan, R. C. (2004). Opposed Migration Aerosol Classifier (OMAC). *Aerosol Sci. Technol.*, 38:890–899.
- Gopalakrishnan, R., and Hogan, C. J. (2012). Coulomb-Influenced Collisions in Aerosols and Dusty Plasmas. *Phys. Rev. E*, 85:026410.
- Gopalakrishnan, R., Meredith, M. R., Larriba-Andaluz, C., and Hogan, C. J. (2013). Brownian Dynamics Determination of the Bipolar Steady State Charge Distribution on Spheres and Non-Spheres in the Transition Regime. *J. Aerosol Sci.*, 63:126–145.
- Gormley, P. G., and Kennedy, M. (1949). Diffusion from a Stream Flowing Through a Cylindrical Tube. *P. Irish Royal Acad.*, 52A:163–169.
- Hering, S. V., and Stolzenburg, M. R. (2005). A Method for Particle Size Amplification by Water Condensation in a Laminar, Thermally Diffusive Flow. *Aerosol Sci. Technol.*, 39:428–436.
- Hering, S. V., Stolzenburg, M. R., Quant, F. R., Oberreit, D. R., and Keady, P. B. (2005). A Laminar-Flow, Water-Based Condensation Particle Counter (WCPC). *Aerosol Sci. Technol.*, 39:659–672.
- Iida, K., Stolzenburg, M. R., McMurry, P. H., Smith, J. N., Quant, F. R., Oberreit, D. R., et al. (2008). An Ultrafine, Water-Based Condensation

- Particle Counter and its Evaluation Under Field Conditions. *Aerosol Sci. Technol.*, 42:862–871.
- Kemmer, G., and Keller, S. (2010). Nonlinear Least-Squares Data Fitting in Excel Spreadsheets. *Nat. Protoc.*, 5:267–281.
- Knutson, E. O., and Whitby, K. T. (1975). Aerosol Classification By Electric Mobility: Apparatus, Theory, and Applications. *J. Aerosol Sci.*, 6:443–451.
- Kulkarni, P., and Wang, J. (2006). New Fast Integrated Mobility Spectrometer for Real-Time Measurement of Aerosol Size Distribution - I: Concept and Theory. *J. Aerosol Sci.*, 37:1303–1325.
- Larriba, C., Hogan, C. J., Attoui, M., Borrajo, R., Fernandez-Garcia, J., and Fernandez de la Mora, J. (2011). The Mobility-Volume Relationship Below 3.0 nm Examined by Tandem Mobility-Mass Measurement. *Aerosol Sci. Technol.*, 45:453–467.
- Martinez-Lozano, P., and Fernandez de la Mora, J. (2006). Resolution Improvements of a Nano-DMA Operating Transonically. *J. Aerosol Sci.*, 37:500–512.
- Mason, E. A., and McDaniel, E. W. (1988). *Transport Properties of Ions in Gases*. Wiley, New York.
- Merenbloom, S. I., Glaskin, R. S., Henson, Z. B., and Clemmer, D. E. (2009). High-Resolution Ion Cyclotron Mobility Spectrometry. *Anal. Chem.*, 81:1482–1487.
- Oberreit, D. R., McMurry, P. H., and Hogan, C. J. (2013). In Prep.
- Revercomb, H. E., and Mason, E. A. (1975). Theory of Plasma Chromatography Gaseous Electrophoresis-Review. *Anal. Chem.*, 47:970–983.
- Rosser, S., and Fernandez de la Mora, J. (2005). Vienna-Type DMA of High Resolution and High Flow Rate. *Aerosol Sci. Technol.*, 39:1191–1200.
- Scheibel, H. G., and Porstendorfer, J. (1983). Generation of Monodisperse Ag-Aerosol and NaCl-Aerosol with Particle Diameters Between 2-nm and 300-nm. *J. Aerosol Sci.*, 14:113–126.
- Song, D. K., and Dhaniyala, S. (2007). Nanoparticle Cross-Flow Differential Mobility Analyzer (NCDMA): Theory and Design. *J. Aerosol Sci.*, 38:964–979.
- St. Louis, R. H., and Hill, H. H. (1990). Ion Mobility Spectrometry in Analytical-Chemistry. *Crit. Rev. Anal. Chem.*, 21:321–355.
- Stolzenburg, M. R. (1988). An Ultrafine Aerosol Size Distribution Measuring System. in *Mechanical Engineering*, University of Minnesota, Minneapolis, MN.
- Stolzenburg, M. R., and McMurry, P. H. (2008). Equations Governing Single and Tandem DMA Configurations and a New Lognormal Approximation to the Transfer Function. *Aerosol Sci. Technol.*, 42:421–432.
- Ude, S., and Fernandez de la Mora, J. (2005). Molecular Monodisperse Mobility and Mass Standards from Electrospays of Tetra-Alkyl Ammonium Halides. *J. Aerosol Sci.*, 36:1224–1237.
- Vidal-de-Miguel, G., Macía, M., and Cuevas, J. (2012). Transversal Modulation Ion Mobility Spectrometry (TM-IMS), A New Mobility Filter Overcoming Turbulence Related Limitations. *Anal. Chem.*, 84:7831–7837.
- Wang, J., McNeill, V. F., Collins, D. R., and Flagan, R. C. (2002). Fast Mixing Condensation Nucleus Counter: Application to Rapid Scanning Differential Mobility Analyzer Measurements. *Aerosol Sci. Technol.*, 36:678–689.
- Wang, S. C., and Flagan, R. C. (1990). Scanning Electrical Mobility Spectrometer. *Aerosol Sci. Technol.*, 13:230–240.
- Wiedensohler, A. (1988). An Approximation of the Bipolar Charge-Distribution for Particles in the Sub-Micron Size Range. *J. Aerosol Sci.*, 19: 387–389.
- Zhang, M., and Wexler, A. S. (2006). Cross Flow Ion Mobility Spectrometry: Theory and Initial Prototype Testing. *Int. J. Mass Spectrom.*, 258: 13–20.